Original manuscript prepared for: bioRxiv

Chronic Intermittent Ethanol Exposure Differentially Alters Microglial Morphology in the Prelimbic Cortex and Nucleus Accumbens Core

Siemsen BM[1,2*], Landin JD[2*], McFaddin JA[1], Hooker KN[1], Chandler LJ[2], & Scofield MD[1,2]

1: Department of Anesthesiology and Perioperative Medicine, Medical University of South Carolina, Charleston, SC, USA

2: Department of Neuroscience, Medical University of South Carolina, Charleston, SC, USA

* indicates these authors contributed equally to this work

Address correspondence to:

Dr. Michael Scofield

Department of Anesthesiology

Medical University of South Carolina

173 Ashley Avenue, Charleston, SC 29425

TEL: 843-792-1743

E-mail: scofield@musc.edu

Number of Words: 5719

Abstract: 235

References: 82

Running title: ETHANOL-INDUCED MICROGLIA ACTIVATION

Keywords: microglia, LPS, Chronic intermittent ethanol, prelimbic cortex, nucleus accumbens

Acknowledgements

This work was supported by R00 DA040004 (MDS), R01 AA010983 (LJC), R01 AA022701 (LJC), and T32 DA007288 (BMS)

Abstract

Chronic intermittent ethanol (CIE) exposure in rats induces neuroplastic adaptations in the prelimbic cortex (PL) and nucleus accumbens core (NAcore) during withdrawal, contributing to deficits in decision-making and escalation of alcohol consumption. Increased evidence has linked neuroplastic changes associated with the development of alcohol dependence and withdrawal to neuroimmune signaling and activation of microglia. Microglia exhibit a well-defined structure/function relationship, with alterations in cytokine release occurring concomitantly with reconfiguration of cellular dimensions and redistribution of fine processes. Accordingly, gaining a better understanding of ethanol-induced microglia activation will provide insight into how neuroimmune signaling may impact neural structure and function following ethanol exposure. The present study characterized CIE-induced alterations in microglia morphology in the PL and NAcore using confocal microscopy and 3D image reconstruction. Rats were sacrificed at peak withdrawal, 10 hours after discontinuation of 15 days of CIE or Air exposure. CIE-exposed rats exhibited an increase in microglia soma size in the PL and NAcore compared to Air-exposed control rats. However, the CIE-mediated increase in soma volume in the PL cortex was accompanied by a reduction in microglial complexity. While systemic LPS elicited similar increases in soma volume in the PL cortex and NAcore, the LPS-induced increase in soma size was associated with increased complexity of microglial processes in the PL cortex, an effect opposite to that of CIE. These data are consistent with the hypothesis that the microglial activation state following CIE is structurally and chemically distinct from the activation state associated with induction of the innate neuroimmune system following systemic LPS exposure.

Introduction

Alcohol use disorders (AUDs) pose a significant public health problem, representing an immense burden to both individuals and to society [1]. Unfortunately, effective treatment for AUDs remains difficult to achieve, and strikingly high relapse rates persist [2, 3]. Given the staggering economic and public health burden of AUDs, there remains a critical need to more completely understand the mechanisms and consequences of alcohol (ethanol) exposure on the brain. In the preclinical setting, rodent models provide valuable tools for understanding the pathophysiological effects of ethanol [4]. Further, rodent models involving chronic intermittent ethanol (CIE) exposure reproduce the somatic symptoms of physical dependence and withdrawal observed in humans [5]. This model also engages neuroplastic alterations that drive escalation of ethanol consumption following CIE, an effect thought to represent the transition from controlled social drinking to uncontrolled compulsive and habitual consumption [4]. The rodent CIE model has also been widely used to elucidate key neuroadaptations in addiction-relevant circuits. For example, craving for ethanol following chronic exposure and protracted withdrawal has been linked to altered glutamatergic plasticity in several key brain regions, including the prelimbic (PL) cortex [6-8] and nucleus accumbens core (NAcore) [9, 10].

Apart from the established link between ethanol-induced neuroplastic changes in neurotransmitter systems such as glutamate, GABA, and dopamine, there is accumulating clinical [11-13] and preclinical [14, 15] evidence for an important role of alterations in glial-mediated neuroimmune activity in the actions of ethanol on brain and behavior. As an example, expression of the canonical microglial marker ionized calcium binding adaptor molecule 1 (Iba-1) is increased in post-mortem brains of alcohol-dependent patients [16]. This has led to the proposal that repeated cycles of exposure to ethanol promotes sensitized responses of the innate immune system [17]. Microglia express several membrane receptors that respond to molecular patterns associated with damage or pathogens. The primary receptors implicated in ethanol's action at microglia are the superfamily of toll-like receptors (TLRs) [18, 19], and the tumor necrosis factor alpha (TNFα) receptor [20]. Further, ethanol exposure during adolescence increases TLR4 expression, and enhances levels of ligands for TLR4 including the damage-associated high-mobility group box 1 (HMGB1) [21]. Yet, it is important to note that the degree to which ethanol leads to TLR4-dependent neurotoxic insult is currently under debate [15, 22-24]. Despite the debate, knock out studies support a TLR4-based mechanism for ethanol's action on microglia, as loss of TLR4 prevents ethanol-induced microglial upregulation in the cortex, and cytokine release in culture [25]. Apart from TLR4, and the TNFα positive feedback loop, ethanol also acts directly on NADPH-oxidase [26], engaging

release of reactive oxygen species linked to alcohol-induced neurodegeneration [27]. Further, microglial inhibitors, including minocycline, have been shown to decrease ethanol self-administration when delivered systemically [28]. Collectively, these data support a role for microglia activation in the ethanol-induced neuroimmune and neuroinflammatory cascades linked to the consequence and maintenance of ethanol drinking.

As Iba-1 is selectively expressed in microglia [29, 30], traditional immunohistochemical labeling and detection of Iba-1 has provided valuable insight into brain region-specific adaptations in microglia structure and proliferation following ethanol exposure. Several studies have shown that chronic ethanol exposure in rats increases the number of Iba-1 positive cells, or increases Iba-1 signal intensity (an early optical marker of microglial activation), in a region-specific manner. For example, while six months of voluntary consumption of a 20% aqueous ethanol solution followed by 2 months of withdrawal did not alter the total number of microglia in the hippocampus, there was an increase in the proportion of activated microglia [22]. Using population studies, it has been reported that 35 days of CIE increased Iba-1 staining intensity in a number of brain regions, including the PFC, an effect that was diminished after 28 days of withdrawal [31]. Further, CIE increases Iba-1 expression in the central amygdala, and this increase is blocked by antagonism of TLR4, a receptor directly linked to ethanol-induced activation of microglia [32]. These findings suggest that CIE exposure induces microglial activation, and thus may play a role in regulation of neuroadaptations associated with chronic ethanol exposure.

Microglia are exceptionally morphologically dynamic [33]. Accordingly, activation-associated alterations in soma size and branching patterns have been systematically characterized, serving as visual biomarkers for neuroimmune activation [34-36]. Recent studies demonstrate brain region-specific heterogeneity in microglial morphology [37], and gene expression profiles [38], supporting the well-established link between structure and function for this unique cell type. Additional careful structural analyses have shown that, even *within* brain regions, individual microglia occupy a broad spectrum of structural properties and consequently, activation states [39]. As such, it has become evident that simple classification of microglia as static, or “resting”, may be inadequate given that microglia constantly survey and respond to the surrounding microenvironment [40]. Indeed, mobile microglial processes traverse the parenchyma at a relatively rapid rate of 1-3 μm per minute [40], influencing synaptic transmission as they sample the interstitial fluid and respond to stimuli with the release of neuromodulators [41]. To date, a systematic analysis of microglia morphological adaptations following

CIE exposure has yet to be comprehensively conducted using high-resolution confocal microscopy and precise digital reconstruction. Here we show that CIE exposure of male rats produces brain region-dependent alterations in microglia morphometric features that display overlapping as well as dichotomous alterations induced by sub-chronic (2-day) immune activation following systemic LPS administration.

Materials and Methods

Subjects

Male Long-Evans rats were obtained from Envigo. Upon arrival, rats were singly housed in standard polycarbonate cages in a temperature-controlled (22˚C) vivarium. Rats were maintained on a 12 hr/12 hr reverse light/dark cycle (lights on at 2100 hours) with *ad libitum* access to food and water throughout the experiment. All experiments were performed in accordance with guidelines for animal care established by National Institutes of Health and approved by MUSC's Institutional Animal Care and Use Committee.

Vapor CIE Exposure

Chronic intermittent ethanol (CIE) exposure was initiated using a well-characterized vapor inhalation model [42]. In brief, adult rats [postnatal day (P) 93] were subjected to 15 consecutive days of ethanol vapor. Each day of exposure consisted of placing rats in standard housing cages into clear acrylic ethanol vapor exposure chambers (Plas Labs; Lansing, MI) for a period of 14 hrs/day. During the 10 hrs out of the chambers, the rats were returned to the animal housing facility. Rats were placed into the chambers at 1800 hours and removed at 0800 hours. Immediately upon removal from the vapor chambers, a 5-point behavioral intoxication scale was utilized to assess the level of intoxication [43]. Immediately prior to placing the rats back into the chambers following the 10 hr ethanol withdrawal period, the severity of withdrawal based upon somatic signs was assess using a 6-point rating system [42, 44]. On every 5th day of exposure, tail blood ($\leq$ 40 µl) was collected immediately upon removal from chambers for subsequent determination of determine blood ethanol concentration (BEC). Air exposed control rats were treated similarly to the CIE exposed rats except they were not placed into the ethanol vapor chambers.

LPS injections

A separate cohort of rats received intraperitoneal injections of 1.0 mg/kg lipopolysaccharides (LPS) from Escherichia coli (Sigma-Aldrich, L2630) in sterile saline (0.9%) once per day for two consecutive days. Rats were then perfused 24 hours after the second injection of LPS.

Immunohistochemistry

Rats were heavily anesthetized with urethane and then transcardially perfused with 120 ml of 0.1M PBS (pH 7.4) followed by 180 ml of freshly prepared 4% paraformaldehyde (PFA) (Fisher Scientific, Hampton NH). Brains were rapidly removed, post-fixed in 4% PFA for 24 hours, and then transferred to 0.1M PBS containing 0.2% sodium azide (w/v) and stored at 4ºC until sectioning. 100 µm thick coronal sections containing the PL cortex (AP 2.76mm – AP 4.2mm from bregma) and the NAcore (AP 1.8mm – AP 0.7mm from bregma) were sliced on a vibrating microtome (Leica Biosystems, VT1000 S) and serial sections were stored in 0.1M PBS with 0.2% sodium azide until processing. PL cortex and NAcore sections were processed for immunohistochemical detection of Iba-1 using 3-4 sections spanning the entirety of the PL cortex and NAcore. Brain sections were blocked in 0.1M PBS containing 2% Triton X-100 (PBST) and 2% normal goat serum (NGS, Jackson Immunoresearch, # 005-000-121) for 2 hours at room temperature with agitation. Sections were then incubated in PBST containing 2% NGS and rabbit anti-Iba-1 (1:1000, Wako #019-19741) primary antisera overnight at 4ºC overnight with agitation. Sections were then washed 3X10 minutes in PBST, then incubated in PBST containing 2% NGS with goat anti-rabbit secondary antisera conjugated to Alexa Fluor® 647 (1:1000, Abcam, Cambridge UK, #A32733) for five hours at room temperature. Sections were then washed 3X10 minutes in PBST, then mounted on superfrost-plus slides with ProLong™ Gold Antifade (Invitrogen, Carlsbad CA, #P36930). Slides were stored at 4ºC until imaging.

High-Resolution Confocal Microscopy

Confocal Z-series image data sets of Iba-1 stained microglia were captured using a Leica SP8 confocal microscope with a 63X (N.A. 1.4) oil-immersion objective. The parameters for imaging acquisition involved two separate modalities. The first set of parameters was designed to image networks of microglia for high throughput analyses of the somatic dimensions. These high throughput data sets were acquired using a diode 638 nm laser line, 2048 x 2048 frame size, 0.75X digital zoom, and a Z-step size of 0.37 µm. The entirety of all visible Iba-1 signal was collected throughout the thickness of the slice (data sets spanning 70-100 µm). The second set of imaging parameters, which were optimized for examining individual microglial cells at high resolution, involved image acquisition using with the same objective and laser line, 2336 x 2336 frame size, 1.5X digital zoom, and a Z-step size of 0.24 µm. Data sets collected with this modality typically spanned 50-70 µm. For single cell microglial imaging, care was taken to ensure that the entirety of the cell was collected in the image by positioning the soma in the middle of the Z-stack during imaging. This ensured that all microglial processes for the cell of

interest, projecting radially and axially, were completely collected. PL microglia were imaged in layer V while those in the NAcore were imaged in the region dorsomedial to the anterior commissure.

Imaris 3D reconstruction and analysis

Following confocal image acquisition, Z-series data sets were imported into Imaris software (Version 9.0, Bitplane, Belfast UK). For high throughput analyses of somatic dimensions, a smooth 3D space-filling model was constructed in order to best fit microglial cell bodies in a semi-automated procedure by an investigator blind to treatment groups. Inaccurate or falsely-recognized somas were adjusted or removed by the investigator. The total number of cells contained within a field as well as each microglial soma volume were analyzed and exported. For individual cell imaging and digital reconstructions, microglia were imaged in their entirety, at higher magnification. The resulting data sets were imported to Imaris for 3D modeling, skeletonization, branching, and Sholl analyses. For single cell data sets, 3D space-filling models of each cell were generated to isolate the individual Iba-1-immunoreactive microglia of interest. Once an individual cell was isolated, the Filament module in Imaris was used to skeletonize each microglia in a semi-automated process. Using the Filament function, the thinnest process diameter was set to 0.5 μm and the overall seed size diameter was set to 8 μm. Each microglia skeletonization was then visually inspected and manually adjusted to best fit the Iba-1 signal. Next, the filament module was combined using a MATLAB plugin to produce a 3D convex hull for each cell. This shape is mathematically defined as the minimum polyhedron that can contain the filament resulting from skeletonization. A 3D convex hull can be used as an index of the territory that each microglia occupy in three dimensions. In our skeletonization analyses, we measured Sholl intersections as a function of distance from cells center (the middle of the soma), convex hull volume (in μm^3), overall cellular volume of microglia (soma and processes), and number of filament branch points. All imaging and analyses were performed by an investigator blinded to experimental groups.

Experimental Design

The timeline for experimental procedures is found in **Figure 1**. The experiment was designed to examine the degree to which CIE alters Iba-1 immunoreactive microglia morphological properties in the PL cortex and NAcore. Rats received CIE for 14 hours a day for 15 days and were sacrificed 10 hours following the final ethanol exposure. The ethanol-naive control rats were handled the same as the ethanol exposed rats with the exception of exposure to ethanol vapor. A separate group of rats received two injections of LPS (1 mg/kg, i.p.) separated by 24 hours, and were sacrificed 24 hours after the

second injection. These animals served as a positive control for microglia activation and were compared to CIE and control rats for each measure.

Statistical Analyses

Statistical analyses were performed using GraphPad Prism software (version 6, GraphPad, San Diego CA). BEC and withdrawal scores were analyzed with a repeated-measures one-way ANOVA followed by Dunnett's multiple comparison test comparing days 10 and 15 to day 5. When three groups were compared across a single dependent variable, a one-way ANOVA was used. Tukey's multiple comparison test was used when a significant effect of treatment (LPS or CIE versus control) was revealed. The number of Sholl's intersections as a function of distance from soma start point was analyzed with a two-way repeated measures ANOVA with treatment (CIE or LPS vs. Naïve) as a between-subjects variable and distance from soma center as a within-subjects variable. Bonferroni-corrected pairwise comparison test was used when a significant interaction was observed. For high-throughput analyses, the average soma volume was calculated for each image for each animal, then animal averages were reported. We also plotted each individual soma volume for each animal in each group as an independent data point to investigate population shifts in microglia soma volume as a function of treatment. Such data were analyzed with a Kolomogorov-Smirnov test; comparing each treatment to every other treatment one test at a time. Data is expressed as the mean +/- the standard error of the mean (SEM)

Results

CIE and LPS exposure differentially alter microglial density and somatic volume

In the present study, we examined microglial morphology in the PL cortex and NAcore of brain slices obtained from three experimental groups of rats: an ethanol-naïve control group, a group of rats that had been subjected to CIE and then sacrificed during the peak of withdrawal (~10 hours into withdrawal) following the last episode of ethanol exposure, and a group of rats that had been injected with LPS once daily for two consecutive days and then sacrificed 24 hours later (**Figure 1**).

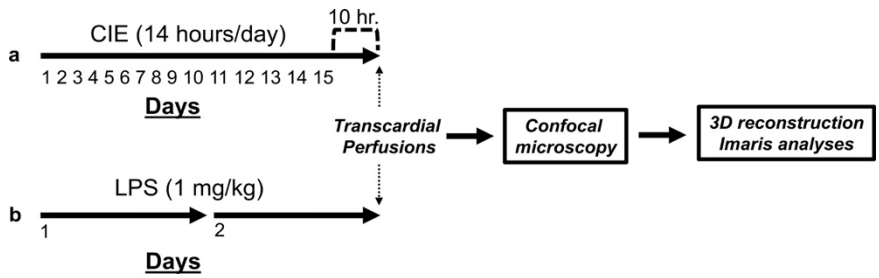

Figure 1. Schematic depiction of the experimental timeline. **a)** Timeline depicting the length of CIE and the sacrifice time-point during withdrawal. **b**) Timeline depicting the number of LPS injections received and the sacrifice time-point following LPS exposure. CIE or LPS treated rats were compared to ethanol-naïve controls on each measure.

For the CIE-exposed group of rats, intoxication and withdrawal scoring were obtained daily while the blood ethanol concentrations (BECs) were measured on 4 separate days of CIE exposure. As shown in **Figure 2A**, the BEC group average across all 4 days was 294.4 +/- 19.67. The corresponding average level of intoxication across all days and all rats was 2.17 +/- 0.09 (**Figure 2B**), which equated to a mild-to-moderate level of intoxication based upon the rating scale. A repeated measures one-way ANOVA comparing withdrawal scores across time in CIE rats showed a significant effect of time ($F(1.8, 7.2)=17.00$, $p<0.01$, **Figure 2C**). Dunnett's multiple comparison test indicated that both day 10 and day 15 exhibited significantly higher withdrawal scores compared to day 5 ($p<0.05$). Specifically, withdrawal scores on day 15 were 2.72 +/-0.56, corresponding with moderate withdrawal. The PL cortex and NAcore represent two key brain regions that undergo neuroadaptations linked to ethanol consumption [9, 45]. In particular, prefrontal cortical dysfunction associated with loss of control over ethanol consumption has been linked to heightened microglia-mediated neuroimmune cascades [16]. Accordingly, confocal imaging of Iba-1 immunohistochemistry was carried out in slices containing the PL (**Figure 2D-F**) and NAcore (**Figure 2G-I)**. As illustrated in the representative images for each region, Iba-1 staining revealed an evenly spaced network of microglial cells with largely non-overlapping fields of highly branched fine processes. Our data is consistent with that of others demonstrating that Iba-1 is a selective marker of microglia [46], and further illustrates that when combined with high-magnification,

high-resolution confocal microscopy, Iba-1 immunostaining can be used for visualizing and analyzing microglial structural properties, including process density and somatic morphology [47].

For investigating the effects of CIE and LPS microglial morphology, the first set of studies focused on analysis of microglial density and on alterations in somatic volume within a defined brain region. In the PL cortex, Iba-1 immunostaining exhibited robust labeling of microglia in slices obtained from control rats (**Figure 3A)**, CIE-exposed rats (**Figure 3B**) and LPS injected rats (**Figure 3C**). Dimensions of the somatic compartment of microglia cells were analyzed using 3D space-filling models, which were color coded to indicate somatic volume in μm^3. Each treatment group consisted of 5 animals. We imaged 4-6 fields of microglia in the PL cortex for a total of 958 cells in the control group, 951 cells in the CIE-exposed animals, and 902 cells in LPS-exposed animals. A one-way ANOVA revealed a significant main effect of treatment on the number of cells/μm^3 ($F(2,12)=5.25$, $p<0.05$). Tukey's multiple comparison test indicated that CIE ($p<0.05$) but not LPS exposure ($p=0.79$) decreased the number of cells/μm^3 when compared to control rats **(Figure 3D)**. A significant main effect of treatment was also observed on the average somatic volume ($F(2,12)=20.61$, $p<0.0001$) (**Figure 3E**). Further, Tukey's multiple comparison tests indicated that, although CIE did not significantly increase microglia soma volume relative to control rats ($p=0.26$), LPS led to a robust increase in soma volume relative to control rats ($p<0.001$) and CIE-exposed rats ($p<0.01$). Cumulative frequency

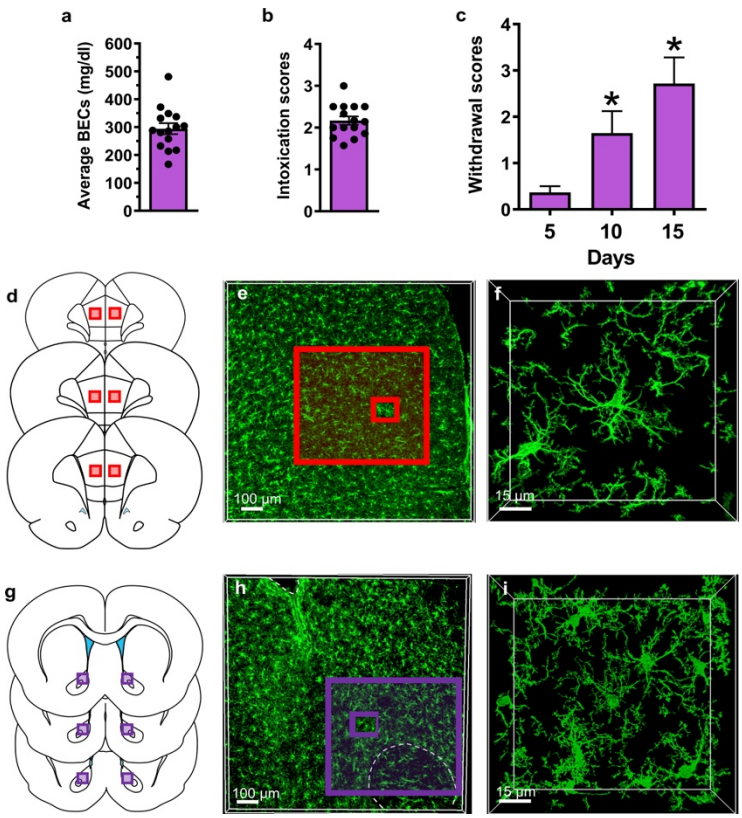

Figure 2. Assessment of ethanol exposure and representative Iba-1 immunohistochemistry in PL cortex and NAcore. **a**) Blood ethanol concentrations (BEC) and **b**) intoxication scores of CIE exposed rats averaged across day 5, 10, and 15 of the CIE exposure period. **c**) Somatic withdrawal scores assessed after 5, 10, and 15 days of CIE exposure (*$p<0.05$ compared to day 5). **d**) The PL subdivision of the medial prefrontal cortex was sampled along the anterior-posterior axis. **e**) Low magnification image of Iba-1 immunoreactivity in the PL cortex. **f**) High magnification image Iba-1 immunoreactive microglia in the PL cortex. The outer red boxed region in **e** represents the area that corresponds to the box region shown in **d,** while the smaller inset red box represents the image area shown in **f**. **g**) The NAcore subdivision of the nucleus accumbens was also sampled from sections across the anterior-posterior axis as described above. **e**) Low magnification images of Iba-1 immunoreactivity in the NAcore. **f**) Higher magnification image of Iba-1 immunoreactive microglia in the NAcore. As above, the outer purple boxed region in **h** represents the area that corresponds to the box region shown in **g** while the smaller inset purple box represents the image area shown in **i**.

distributions of microglial somata using each microglia in each image as an independent data point were also generated as shown in **Figure 3F**. Comparison of the microglial soma volume frequency distribution in the PL cortex of CIE exposed rats to the frequency distribution in control rats revealed a significant rightward shift in the somatic volume distribution (K-S D=0.13, $p<0.0001$). This effect was even more pronounced for LPS-exposed rats in comparison to control (K-S D=0.31, $p<0.0001$) and to CIE-exposed rats (K-S D=0.20, $p<0.0001$).

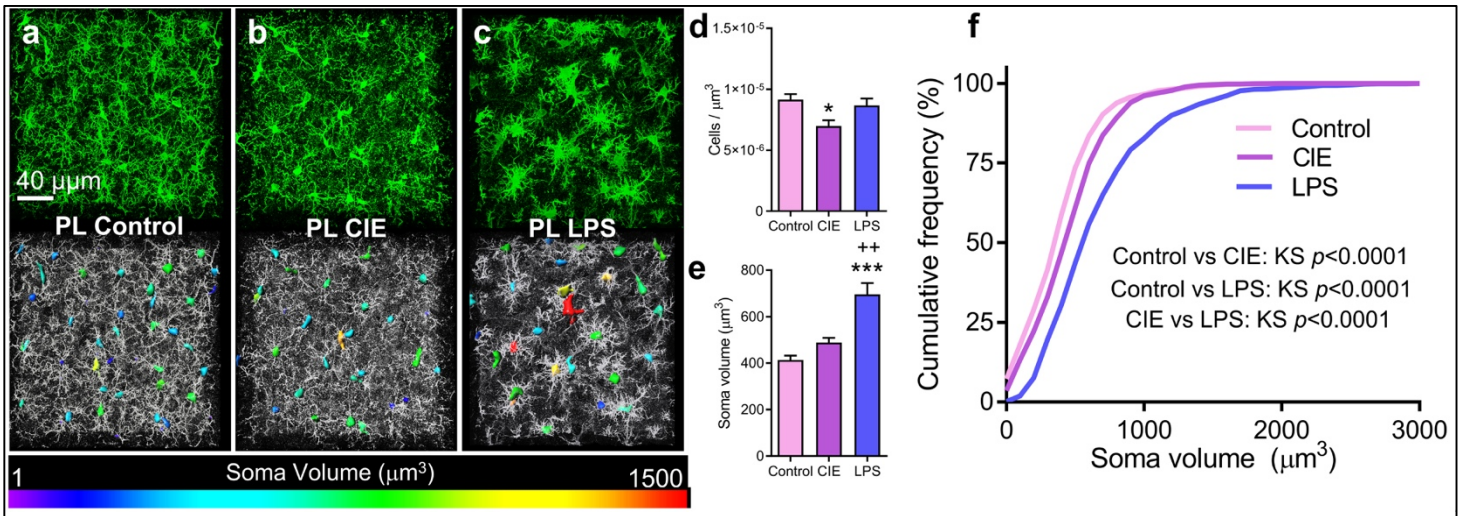

Figure 3. Both CIE and LPS exposure resulted in an increase in somatic volume of microglia in the PL cortex. Representative Iba-1 staining of microglia in the PL cortex for control (**a**), CIE-exposed (**b**), and LPS-exposed (**c**) rats. Somas are color-coded to indicate the spectrum of soma volumes observed for each treatment. **d**) CIE exposure reduced the number of Iba-1 immunoreactive microglia per micron^3 in the PL cortex. **e**) LPS (but not CIE) exposure was associated with a significant increase in the somatic volume when compared to control rats. **f**) Examination of the frequency distribution of somatic volume revealed that both CIE and LPS exposure resulted in a rightward shift in soma volume distribution curve. *$p<0.05$, ***$p<0.001$ compared to control; ++$p<0.01$ compared to CIE.

Iba-1 Immunostaining revealed a similar microglial syncytium in the NAcore (**Figure 4A-C**). As above, each group consisted of the same five animals used in the PL imaging. As with the PL, we imaged 4-6 fields of microglia per animal for a total of 929 total cells in control rats, 833 total cells in CIE-exposed rats, and 942 total cells in LPS-exposed rats. Analysis of the immunostaining in the NAcore of the three experimental groups of rats again yielded a significant main effect of treatment on the number of cells per µm^3 when collapsed across animals ($F(2,12)=6.72$, $p<0.05$). Tukey's multiple comparison test indicated that LPS exposure ($p<0.05$), but not CIE exposure ($p=0.29$), reduced the number of cells per µm^3, when compared to control rats (**Figure 4D**), an effect that was opposite to that observed in the PL cortex. Also akin to observations in the PL cortex, there was a significant main effect of treatment on the average soma volume ($F(2,12)=17.43$, $p<0.001$). Tukey's multiple comparison test indicated that LPS exposure resulted in a significant increase in the average microglia soma volume compared to

control rats (p<0.001) as well as CIE-exposed rats (p<0.01, **Figure 4E**). The 3D renderings of microglia somata in the NAcore was next examined using cumulative frequency distributions. Comparison of CIE-exposed rats to control rats revealed a significant rightward shift in the somatic volume distribution (K-S D=0.09, p<0.01). As shown in Figure 4F, LPS exposure was again associated with a dramatic rightward shift in the somatic volume frequency distribution of microglia in the NAcore compared to control (K-S D=0.32, p<0.0001) and CIE (K-S D=0.24, p<0.0001).

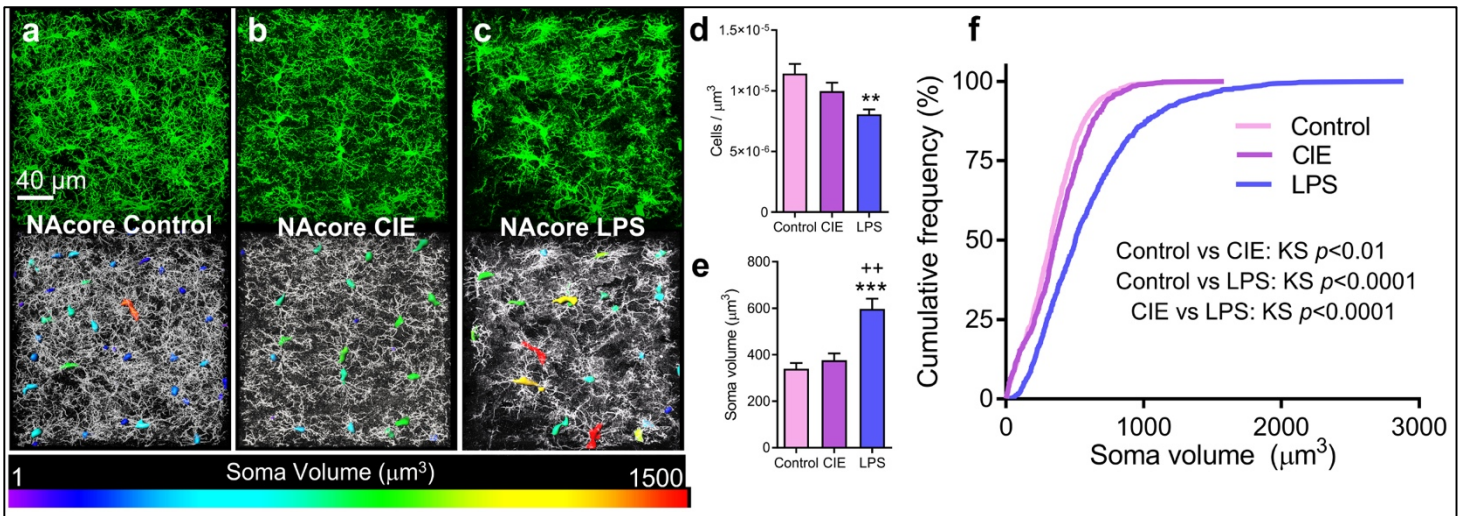

Figure 4. CIE and LPS exposure resulted in an increase in somatic volume of microglia in the NAcore**. a**) Representative Iba-1 staining of microglia in the NAcore of control, (**b**) CIE, and (**c**) LPS-exposed rats. Somas are color-coded to indicate the spectrum of soma volumes observed for each treatment. **d**) LPS-exposed rats exhibited a reduction in the number of Iba-1 immunoreactive microglia per micron^3 in the NAcore. **e**) When soma volume was averaged across all images for each animal, only LPS significantly increased the soma volume compared to control rats. **f**) Examination of the frequency distribution of somatic volume revealed that both CIE and LPS exposure resulted in a rightward shift in soma volume distribution curve. *p<0.05, ***p<0.001 compared to control; ++p<0.01 compared to CIE.

Dichotomous changes in microglial morphology and complexity following CIE and LPS exposure

As opposed to the population approach used for analysis of microglial density and somatic volume, we utilized a high magnification single-cell imaging modality to precisely map microglia structural patterns following CIE or LPS exposure. As shown in the representative images in **Figure 5A-C** Iba-1 was used to label individual microglia in the PL. The complexity of microglial arbors was then assessed using a 3D Sholl sphere analysis, with concentric spheres placed at 1 µm intervals from the center of the skeleton. This analysis revealed a significant treatment by distance interaction for LPS compared to control rats (F(49,392)=3.981, p<0.0001) (**Figure 5D**). Further, Bonferroni-corrected pairwise comparison tests indicated that LPS treated rats had a significantly greater number of Sholl sphere breaks at 11-14 µm from the center of the cell (p<0.05). However, there was no significant treatment

by distance interaction of the number of intersections for CIE-exposed versus control rats (F(49,392)=1.16, *p*=0.21).

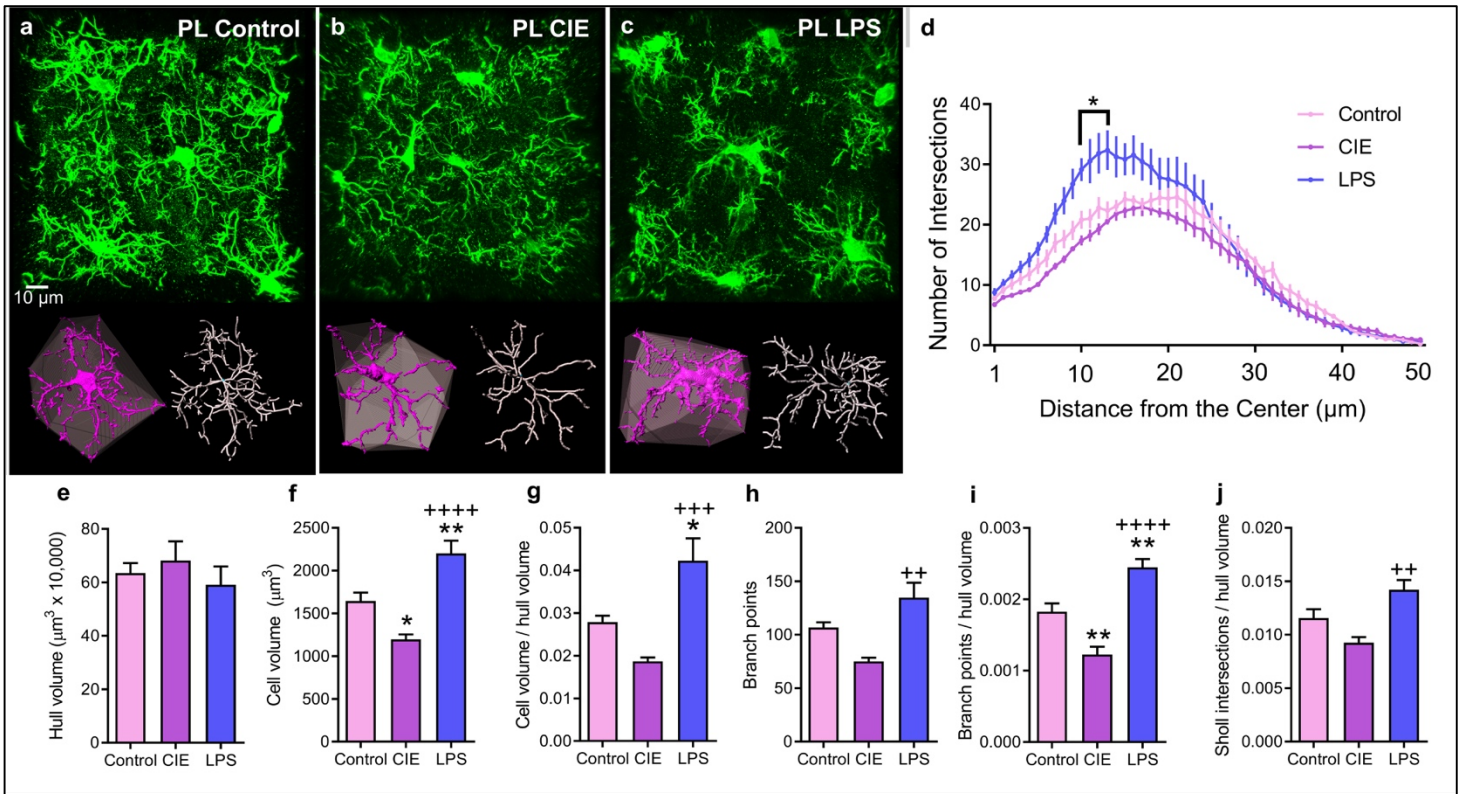

Figure 5. CIE and LPS exposure resulted in dichotomous alterations in microglia complexity in the PL cortex. **a-c**) Raw data (green), digitized single cells (purple) and associated convex hulls (grey), as well as skeletonizations (white) for PL cortex microglia in (**a**) control, (**b**) CIE-exposed, and (**c**) LPS-exposed rats. **d**) Sholl's analysis revealed that LPS exposure resulted in a greater number of breaks (in 1 µm intervals) closer to the center of the cell compared to control rats. **e**) There was no difference between groups in the average territory occupied by microglia ('Hull' volume). **f**) CIE exposure reduced while LPS exposure increased the average volume of microglia. **g**) When normalized to the hull volume, the reduction in volume following the CIE exposure was lost while the LPS-induced increased in volume was still observed. **h**) There was no effect of CIE or LPS on the number of branch points compared to control rats, yet LPS increased branching when compared to CIE. **(i)** When normalized to the convex hull volume, CIE exposure decreased while LPS increased the number of branch points. **j**) When normalized to the hull volume, there was no effect of CIE or LPS in the number of Sholl intersections compared to control rats in the PL cortex, yet LPS was significantly different compared to CIE. **p*<0.05, ***p*<0.01 compared to control; ++*p*<0.01, +++ *p*<0.001, ++++ *p*<0.0001 compared to CIE.

Following skeletonization of the microglia processes, an associated convex hull, or representation of the spatial territory that each microglia occupies, was generated. Polygonal convex hull renderings estimate the territory individual cells occupy, and can be used to normalize measures of cellular morphological complexity [35]. Accordingly, several indices of microglia architecture were analyzed independent and dependent of convex hull volume in μm^3. Our analyses revealed that there was no difference between groups in the average hull volume of individual microglia in the PL cortex

($F(2,12)=0.55$, $p=0.58$, **Figure 5E**). However, there was a significant main effect of treatment on microglial cell volume ($F(2,12)=22$, $p<0.0001$). As shown in **Figure 5F**, Tukey's multiple comparison test revealed that microglia in the PL of CIE-exposed rats had significantly lower overall cellular volume compared to the control group ($p<0.05$). In contrast, LPS-exposed rats exhibited significantly larger overall cellular volume compared to controls ($p<0.01$) and CIE-exposed rats ($p<0.0001$). Normalization of microglia cell volume to convex hull volume (a description of the density of the microglial process field) also revealed a significant main effect of treatment ($F(2,12)=13.97$, $p<0.001$) (**Figure 5G**). Tukey's multiple comparison tests indicated that LPS exposure significantly increased the microglial density compared to control ($p<0.05$) and CIE-exposed rats ($p<0.001$), whereas CIE exposure did not alter density when compared to control rats ($p=0.14$). Another parameter used to describe microglial structure and complexity is the degree and extent of process branching. Examination of the number of branch points for each microglia revealed a significant main effect of treatment ($F(2,12)=11.58$, $p<0.01$) (**Figure 5H**). Tukey's multiple comparison test indicated that compared to control rats neither LPS ($p=0.10$) or CIE ($p=0.06$) treatment impacted the number of microglial branch points, although both were marginally significant. However, LPS increased the number of branch points compared to CIE-exposed rats ($p<0.01$). As shown in **Figure 5I**, normalization of the number of branch points to convex hull volume also revealed a main effect of treatment ($F(2,12)=29.02$, $p<0.0001$). Tukey's multiple comparison test of the normalized branch data now indicated that CIE exposure resulted in a reduction of branch points per micron of microglia hull volume ($p<0.01$), whereas LPS-exposed rats exhibited an increase in the number of branch points normalized to the hull volume when compared to both control ($p<0.01$) and CIE-exposed rats ($p<0.0001$). As a final measure of complexity, normalization of the total number of Sholl intersections to convex hull volume revealed a significant main effect of treatment ($F(2,12)=10.53$, $p<0.01$). Tukey's multiple comparison test indicated that neither CIE ($p=0.13$) or LPS ($p=0.07$) exposure significantly decreased the number of Sholl intersections when normalized to the hull volume compared to control rats, whereas LPS exposure increased the number of intersections normalized to hull volume compared to CIE rats ($p<0.01$, **Figure 5J**).

The single cell structural analysis approach was used to assess changes in the cellular complexity of microglia in the NAcore. Representative confocal images of the microglia in the NAcore for the three experimental groups are presented in **Figure 6A-C**. As was observed with microglia in the PL cortex, there was a significant treatment by distance interaction in the number of Sholl intersections in LPS-exposed rats compared to control rats ($F(49,392)=8.78$, $p<0.0001$) (**Figure 6D**). Bonferroni-corrected pairwise comparison tests indicated that LPS exposure significantly increased the number of Sholl

intersections at 11-14 and 16-23 microns from the center of the cell ($p<0.05$). Although there was a significant treatment by distance interaction in the number of Sholl intersections in CIE compared to control rats ($F(49,392)=1.49$, $p<0.05$), Bonferroni-corrected pairwise comparison tests indicated no significant differences between CIE and control.

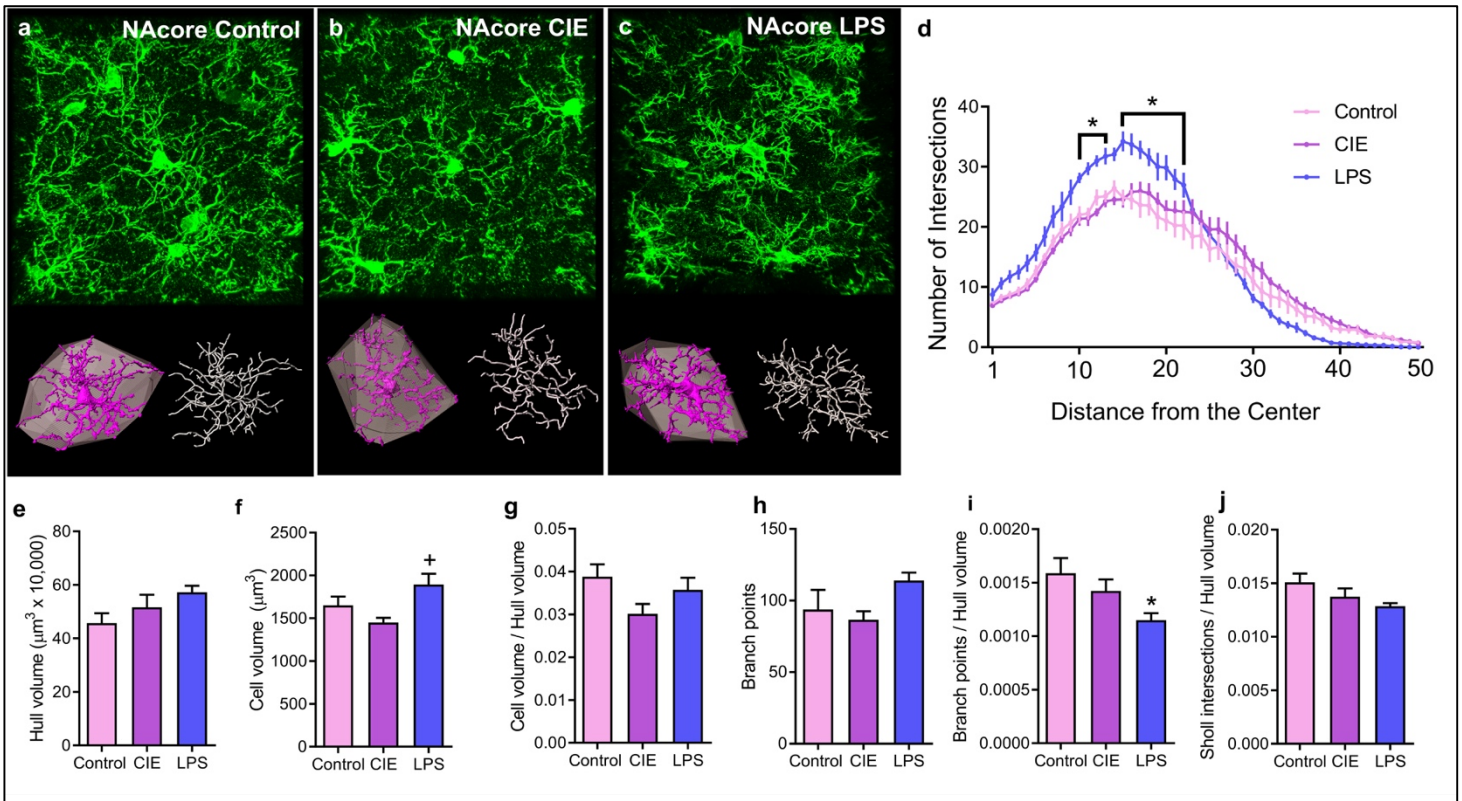

Figure 6. Differential effects of CIE and LPS on microglial complexity were not observed in the NAcore. **a-c**) Raw data (green), digitized single cells (purple) and associated convex hulls (grey), as well as skeletonizations (white) for NAcore microglia in (**a**) control (**b**) CIE-exposed and (**c**) LPS-exposed rats. **d**) Sholl analysis revealed that LPS-exposure resulted in a greater number of breaks (in 1 µm intervals) closer to the center of the cell compared to control rats. **e**) There was no difference between groups in the microglia convex hull volume in the NAcore. **f**) Neither CIE nor LPS exposure affected microglial volume in the NAcore compared to control. There was no difference between groups in microglia cell volume normalized to the volume of territory occupied (**g**) or **h**) the number of branch points. **i**) Uniquely, in the NAcore LPS exposure significantly decreased the number of branch points normalized to the volume of territory occupied when compared to control rats. **j**) The number of Sholl intersections normalized to the hull volume was not different between groups in the NAcore. *$p<0.05$ compared to control; +$p<0.05$ compared to CIE.

Analysis of the convex hull volume in the NAcore (**Figure 6E**) revealed there were no significant group differences ($F(2,12)=2.377$, $p=0.13$), while analysis of microglial cell volume (**Figure 6F**) indicated a significant main effect of treatment ($F(2,12)=5.21$, $p<0.05$). However, Tukey's multiple comparison test indicated a significant difference between CIE and LPS-exposed rats ($p<0.05$) but no significant

difference for either CIE (p=0.34) or LPS (p=0.22) was compared to control. There was no significant effect of treatment ($F(2,12)=2.71$, p=0.10) (**Figure 6G**) when the microglia volume was normalized to the convex hull volume, or for the number of branch points ($F(2,12)=2.38$, p=0.13, **Figure 6H**). However, the number of branch points normalized to hull volume exhibited a significant difference between groups ($F(2,12)=4.159$, $p<0.05$, **Figure 6I**). Tukey's multiple comparison test indicated that LPS ($p<0.05$), but not CIE (p=0.54), significantly decreased the number of branch points normalized to hull volume compared to control rats. Moreover, or the number of Sholl intersections normalized to convex hull volume was not significantly different between groups ($F(2,12)=2.77$, p=0.10, **Figure 6J**).

Discussion

The results of the current study demonstrate that CIE exposure alters the morphological profile of microglia in a manner that is consistent with activation. Specifically, rats that were rendered physically dependent to ethanol by 15 days of CIE exposure, then sacrificed during the peak of withdrawal hyperexcitability, exhibited a significant increase in somatic volume relative to the ethanol-naive control rats. This increase was observed in both the PL and NAcore, two core brain regions of the addiction neurocircuitry [45, 48]. In comparison, rats that were exposed to a 2-day sub-chronic regimen of LPS, known to promote activation and morphological changes in microglia [49], displayed a significantly greater increase in their somatic volume, when compared to the effects of CIE exposure and withdrawal. Confocal analyses of the fine process fields of individual microglia revealed that CIE and LPS exposure induced divergent changes in cellular morphology. While LPS exposure significantly increased various indices of microglial complexity, including branching and process density, microglia in slices from CIE-exposed rats exhibited a reduction in branching and process density. Collectively, these data suggest that while both LPS and CIE exposure lead to activation of microglia, they produce dichotomous alterations in microglial structure at the single cell level that may reflect unique aspects of the correspondingly distinct pathophysiologies.

Comparing CIE and withdrawal- and LPS-mediated microglial activation.

Microglia activation has been implicated in the regulation of the neural processes linked to cognition, memory, and associative learning, as well as neuroplasticity and neuropathology associated with acute and chronic exposure to alcohol [25, 50-54]. Both ethanol and LPS promote microglial activation via TLR4 resulting in the release of a variety of neuromodulators including the proinflammatory cytokine TNFα [23, 25]. Further, TNFα release is responsible for activation of neuroinflammatory signaling cascades following chronic ethanol exposure [24]. In an effort to discard binary classification of microglia as ‘active’ or ‘inactive’ [55], an emerging theory posits that ethanol exposure produces a state of “partial activation” in microglia [15, 26]. As described above, here we report that CIE produces a subtle rightward shift in microglia soma volume in the PL cortex and NAcore, consistent with partial activation. Supporting the partial activation hypothesis, 6 months of ethanol exposure increased the proportion of activated microglia relative to total microglia in the hippocampus without impacting TNFα expression [22]. In addition, binge-like alcohol exposure during adolescence elicits increased CD11b immunoreactivity in the hippocampus, a measure of microglial activation [56], without affecting TNFα expression [15].

Acute exposure to LPS by intraperitoneal injection has been shown to induce the release of proinflammatory cytokines within 2-4 hours [49]. As microglia are exceptionally structurally dynamic [57], and LPS is a potent inducer of microglial activation [58], it is not surprising that the duration and extent of LPS treatment has a profound impact on the structural manifestation of microglial activation [59]. In the present study, we observed that two injections of LPS at 1mg/kg administered 24 hours apart produced a dramatic increase in the size of microglia soma, when compared to control rats or what was seen with CIE, in both the PL and NAcore. This observation is also consistent with stronger, or more pronounced, microglia activation following LPS exposure when compared to CIE and withdrawal [36]

Interestingly, at the single cell level, our structural analyses demonstrate opposing effects of LPS and CIE on microglia architecture. Thus, LPS- and CIE-mediated microglial activation could be mechanistically distinct. In support of this hypothesis, binge alcohol exposure during adolescence leads to increased microglia proliferation during adulthood, independent of phagocytic activity or increased MHC-II expression commonly associated with 'activated' microglia [60]. Accordingly, ethanol-induced microglia activation is likely independent of the innate immune reaction observed in microglia following LPS treatment (i.e. upregulation of MHC-II) [61]. We propose that the unique aspects of CIE- or LPS-induced pathophysiology are reflected by distinct morphological profiles and, potentially, cytokine release patterns.

Brain region-specific effects of CIE and LPS on microglia complexity

At a global level, the frontal cortex and nucleus accumbens show distinct patterns of gene expression in alcoholic patients. As an example, within the genes identified as "alcohol-responsive", only 6% are shared between the prefrontal cortex and nucleus accumbens [63]. Speaking to these brain region-specific effects, CIE in rats produces a greater degree of "alcohol-responsive" genes in the PL cortex when compared to the NAcore [64]. These findings resonate well with data presented here demonstrating reductions in PL microglia branching, a metric of microglial activation commonly observed in response to injury [65], that are largely absent in the NAcore. Given that microglia play an important role in shaping synaptic plasticity by sampling the microenvironment and releasing and responding to cytokines and other neuroimmune modulators [66], neural circuit dysfunction following chronic ethanol exposure likely involves differential morphological and functional adaptations of microglia in the PL cortex and NAcore.

When focusing on single cell architecture, LPS increased complexity of microglia in the PL and NAcore, as indicated by Sholl analyses. However, LPS increased the number of branch points as well as the

density of microglia processes within individual cellular territories, specifically in the PL cortex and not the NAcore. Taken together, our data are largely consistent with the generally bushy, condensed 'deramified' structural pattern reported following LPS-mediated microglia activation [49]. However, our LPS treatment regimen did not produce amoeboid microglia, a structural profile associated with activation of microglia during neurodegeneration [67, 68]. Specifically, the structural pattern we observed following LPS exposure is reminiscent of the previously-identified hyper-ramification morphological profile, a morphological profile characterized by both an enlarged soma and increased branching and branch density[35]. Specifically, the greater number of Sholl intersections closer to the center of the cell and increased branch points in PL microglia could be interpreted as hyper-ramification. Activated microglia that display the hyper-ramified structural profile have also been observed following chronic stress [69], ischemic stroke [65] and traumatic brain injury [35]. Considering the ongoing revisions to the cellular, molecular, and structural characteristics associated with microglia activation [55], the use of high resolution microscopy and digital reconstruction is poised to provide new structural biomarkers that can be used to better understand how alterations in complexity relate to aspects of microglial activation.

A potential role for microglia in regulating corticostriatal glutamatergic signaling

Microglia shape neuronal communication through cytokine release and neuroimmune signaling, with disruptions of these processes described in several pathological conditions [41, 72, 73]. LPS has been shown to result in microglia activation in the cortex 2 days after an acute peripheral injection, yet impacts on dendritic spine turnover are not observed until 56 days after injection [74]. In contrast, CIE in rats leads to a preferential increase in the density of mushroom spines on basal dendrites, and concomitant increase in the NMDA component of evoked glutamate currents in layer V PL pyramidal neurons. Further, CIE increases the expression of NR1 and NR2B NMDA receptor subunits in the PL cortex [6]. In accordance with the well-established role for bidirectional communication between microglia and neurons in the regulation of neuronal structural and synaptic plasticity [75-77], microglia-mediated TNFα release increases NR1 surface expression, NMDA-mediated Ca^{2+} influx, and evokes excitatory post-synaptic currents in hippocampal neurons [78]. Taken together, these data potentially support a role for altered microglial signaling in the manifestation of CIE-induced alterations in cortical plasticity. Moreover, microglial release of TNFα acts as a potent regulator of synaptic scaling, a phenomenon that can be described as an increase or decrease in single-cell synaptic strength or excitability in response to circuit-wide neuronal activity [79]. Interestingly, microglial regulation of synaptic scaling is thought to be engaged by altering astrocyte-mediated activation of metabotropic glutamate receptors [80], a cellular

mechanism linked to relapse vulnerability across several drugs of abuse [81, 82]. Accordingly, interactions between microglia, astroglia, and neurons likely contribute to the altered neuronal plasticity following CIE. Undoubtedly, a greater understanding of the mechanisms underlying CIE-induced alteration in synaptic communication will be garnered through experiments designed to take all three cell types into consideration.

Conclusion and future directions

In summary, population-level cellular analyses reveal a brain-region independent effect of CIE and LPS on microglia soma dimensions, while single cell-level analyses indicated dichotomous effects of these two treatments on microglia activation, observed specifically in the PL cortex and not the NAcore. Further, the impact of CIE on microglia morphology and complexity was relegated largely to the PL cortex. We posit that the methods and results presented here lay a framework for high fidelity 3D structural characterization and classification of microglia following distinct environmental insults, and that usage of the methods described here will allow us to gain a better understanding of the scope of microglial diversity through high order structural characterization and classification.

Compliance with ethical standards

The authors declare that they have no conflict of interest.

All procedures performed in studies involving animals were in accordance with the ethical standards of the institution or practice at which the studies were conducted. This article does not contain any studies with human participants.

References:

1. Kranzler HR, Soyka M. Diagnosis and Pharmacotherapy of Alcohol Use Disorder: A Review. *JAMA.* 2018;320(8): 815-824

2. Rinck M, Wiers RW, Becker ES, Lindenmeyer J. Relapse prevention in abstinent alcoholics by cognitive bias modification: Clinical effects of combining approach bias modification and attention bias modification. *J Consult Clin Psychol.* 2018;86(12): 1005-1016

3. Blaine SK, Sinha R. Alcohol, stress, and glucocorticoids: From risk to dependence and relapse in alcohol use disorders. *Neuropharmacology.* 2017;122: 136-147.PMC5479733

4. Hopf FW, Lesscher HM. Rodent models for compulsive alcohol intake. *Alcohol.* 2014;48(3): 253-264.PMC4993047

5. Gilpin NW, Richardson HN, Cole M, Koob GF. Vapor inhalation of alcohol in rats. *Curr Protoc Neurosci.* 2008;Chapter 9: Unit 9 29.PMC2583102

6. Kroener S, Mulholland PJ, New NN, Gass JT, Becker HC, Chandler LJ. Chronic alcohol exposure alters behavioral and synaptic plasticity of the rodent prefrontal cortex. *PLoS One.* 2012;7(5): e37541.PMC3364267

7. Griffin WC, 3rd, Haun HL, Hazelbaker CL, Ramachandra VS, Becker HC. Increased extracellular glutamate in the nucleus accumbens promotes excessive ethanol drinking in ethanol dependent mice. *Neuropsychopharmacology.* 2014;39(3): 707-717.PMC3895249

8. Griffin WC, Ramachandra VS, Knackstedt LA, Becker HC. Repeated cycles of chronic intermittent ethanol exposure increases basal glutamate in the nucleus accumbens of mice without affecting glutamate transport. *Front Pharmacol.* 2015;6: 27.PMC4337330

9. Das SC, Yamamoto BK, Hristov AM, Sari Y. Ceftriaxone attenuates ethanol drinking and restores extracellular glutamate concentration through normalization of GLT-1 in nucleus accumbens of male alcohol-preferring rats. *Neuropharmacology.* 2015;97: 67-74.PMC4537362

10. Gass JT, Olive MF. Glutamatergic substrates of drug addiction and alcoholism. *Biochem Pharmacol.* 2008;75(1): 218-265.PMC2239014

11. Beech RD, Qu J, Leffert JJ, et al. Altered expression of cytokine signaling pathway genes in peripheral blood cells of alcohol dependent subjects: preliminary findings. *Alcohol Clin Exp Res.* 2012;36(9): 1487-1496.PMC3393821

12. Manzardo AM, Poje AB, Penick EC, Butler MG. Multiplex Immunoassay of Plasma Cytokine Levels in Men with Alcoholism and the Relationship to Psychiatric Assessments. *Int J Mol Sci.* 2016;17(4): 472.PMC4848928

13. Devalaraja MN, McClain CJ, Barve S, Vaddi K, Hill DB. Increased monocyte MCP-1 production in acute alcoholic hepatitis. *Cytokine.* 1999;11(11): 875-881

14. McClain JA, Hayes DM, Morris SA, Nixon K. Adolescent binge alcohol exposure alters hippocampal progenitor cell proliferation in rats: effects on cell cycle kinetics. *J Comp Neurol.* 2011;519(13): 2697-2710.PMC3454493

15. Marshall SA, McClain JA, Kelso ML, Hopkins DM, Pauly JR, Nixon K. Microglial activation is not equivalent to neuroinflammation in alcohol-induced neurodegeneration: The importance of microglia phenotype. *Neurobiol Dis.* 2013;54: 239-251.PMC3629000

16. He J, Crews FT. Increased MCP-1 and microglia in various regions of the human alcoholic brain. *Exp Neurol.* 2008;210(2): 349-358.PMC2346541

17. Crews FT, Lawrimore CJ, Walter TJ, Coleman LG, Jr. The role of neuroimmune signaling in alcoholism. *Neuropharmacology.* 2017;122: 56-73.PMC5493978

18. Liu D, Wang Z, Liu S, Wang F, Zhao S, Hao A. Anti-inflammatory effects of fluoxetine in lipopolysaccharide(LPS)-stimulated microglial cells. *Neuropharmacology.* 2011;61(4): 592-599

19. Crews FT, Walter TJ, Coleman LG, Jr., Vetreno RP. Toll-like receptor signaling and stages of addiction. *Psychopharmacology (Berl).* 2017;234(9-10): 1483-1498.PMC5420377

20. Flores-Bastias O, Karahanian E. Neuroinflammation produced by heavy alcohol intake is due to loops of interactions between Toll-like 4 and TNF receptors, peroxisome proliferator-activated receptors and the central melanocortin system: A novel hypothesis and new therapeutic avenues. *Neuropharmacology.* 2018;128: 401-407

21. Crews FT, Vetreno RP. Mechanisms of neuroimmune gene induction in alcoholism. *Psychopharmacology (Berl).* 2016;233(9): 1543-1557.PMC4828484

22. Cruz C, Meireles M, Silva SM. Chronic ethanol intake induces partial microglial activation that is not reversed by long-term ethanol withdrawal in the rat hippocampal formation. *Neurotoxicology.* 2017;60: 107-115

23. Bi XL, Yang JY, Dong YX, et al. Resveratrol inhibits nitric oxide and TNF-alpha production by lipopolysaccharide-activated microglia. *Int Immunopharmacol.* 2005;5(1): 185-193

24. Alfonso-Loeches S, Pascual-Lucas M, Blanco AM, Sanchez-Vera I, Guerri C. Pivotal role of TLR4 receptors in alcohol-induced neuroinflammation and brain damage. *J Neurosci.* 2010;30(24): 8285-8295

25. Fernandez-Lizarbe S, Pascual M, Guerri C. Critical role of TLR4 response in the activation of microglia induced by ethanol. *J Immunol.* 2009;183(7): 4733-4744

26. Yang JY, Xue X, Tian H, et al. Role of microglia in ethanol-induced neurodegenerative disease: Pathological and behavioral dysfunction at different developmental stages. *Pharmacol Ther.* 2014;144(3): 321-337

27. Qin L, Crews FT. NADPH oxidase and reactive oxygen species contribute to alcohol-induced microglial activation and neurodegeneration. *J Neuroinflammation.* 2012;9: 5.PMC3271961

28. Agrawal RG, Hewetson A, George CM, Syapin PJ, Bergeson SE. Minocycline reduces ethanol drinking. *Brain Behav Immun.* 2011;25 Suppl 1: S165-169.PMC3098317

29. Ito D, Imai Y, Ohsawa K, Nakajima K, Fukuuchi Y, Kohsaka S. Microglia-specific localisation of a novel calcium binding protein, Iba1. *Brain Res Mol Brain Res.* 1998;57(1): 1-9

30. Ahmed Z, Shaw G, Sharma VP, Yang C, McGowan E, Dickson DW. Actin-binding proteins coronin-1a and IBA-1 are effective microglial markers for immunohistochemistry. *J Histochem Cytochem.* 2007;55(7): 687-700

31. Sanchez-Alavez M, Nguyen W, Mori S, et al. Time course of microglia activation and brain and blood cytokine/chemokine levels following chronic ethanol exposure and protracted withdrawal in rats. *Alcohol.* 2018;76: 37-45

32. Bajo M, Montgomery SE, Cates LN, et al. Evaluation of TLR4 Inhibitor, T5342126, in Modulation of Ethanol-Drinking Behavior in Alcohol-Dependent Mice. *Alcohol Alcohol.* 2016;51(5): 541-548.PMC5004745

33. Avignone E, Lepleux M, Angibaud J, Nagerl UV. Altered morphological dynamics of activated microglia after induction of status epilepticus. *J Neuroinflammation.* 2015;12: 202.PMC4634193

34. Fernandez-Arjona MDM, Grondona JM, Granados-Duran P, Fernandez-Llebrez P, Lopez-Avalos MD. Microglia Morphological Categorization in a Rat Model of Neuroinflammation by Hierarchical Cluster and Principal Components Analysis. *Front Cell Neurosci.* 2017;11: 235.PMC5550745

35. Morrison H, Young K, Qureshi M, Rowe RK, Lifshitz J. Quantitative microglia analyses reveal diverse morphologic responses in the rat cortex after diffuse brain injury. *Sci Rep.* 2017;7(1): 13211.PMC5643511

36. Davis BM, Salinas-Navarro M, Cordeiro MF, Moons L, De Groef L. Characterizing microglia activation: a spatial statistics approach to maximize information extraction. *Sci Rep.* 2017;7(1): 1576.PMC5431479

37. Olah M, Biber K, Vinet J, Boddeke HW. Microglia phenotype diversity. *CNS Neurol Disord Drug Targets.* 2011;10(1): 108-118

38. Grabert K, Michoel T, Karavolos MH, et al. Microglial brain region-dependent diversity and selective regional sensitivities to aging. *Nat Neurosci.* 2016;19(3): 504-516.PMC4768346

39. Harry GJ, Kraft AD. Microglia in the developing brain: a potential target with lifetime effects. *Neurotoxicology.* 2012;33(2): 191-206.PMC3299893

40. Nimmerjahn A, Kirchhoff F, Helmchen F. Resting microglial cells are highly dynamic surveillants of brain parenchyma in vivo. *Science.* 2005;308(5726): 1314-1318

41. Kettenmann H, Kirchhoff F, Verkhratsky A. Microglia: new roles for the synaptic stripper. *Neuron.* 2013;77(1): 10-18

42. Trantham-Davidson H, Burnett EJ, Gass JT, et al. Chronic alcohol disrupts dopamine receptor activity and the cognitive function of the medial prefrontal cortex. *The Journal of neuroscience : the official journal of the Society for Neuroscience.* 2014;34(10): 3706-3718.PMC3942586

43. Gass JT, Glen WB, Jr., McGonigal JT, et al. Adolescent alcohol exposure reduces behavioral flexibility, promotes disinhibition, and increases resistance to extinction of ethanol self-administration in adulthood. *Neuropsychopharmacology.* 2014;39(11): 2570-2583.PMC4207336

44. Nixon K, Crews FT. Binge ethanol exposure decreases neurogenesis in adult rat hippocampus. *Journal of neurochemistry.* 2002;83(5): 1087-1093

45. George O, Sanders C, Freiling J, et al. Recruitment of medial prefrontal cortex neurons during alcohol withdrawal predicts cognitive impairment and excessive alcohol drinking. *Proc Natl Acad Sci U S A.* 2012;109(44): 18156-18161.PMC3497825

46. Shapiro LA, Perez ZD, Foresti ML, Arisi GM, Ribak CE. Morphological and ultrastructural features of Iba1-immunolabeled microglial cells in the hippocampal dentate gyrus. *Brain Res.* 2009;1266: 29-36.PMC2677570

47. Kozlowski C, Weimer RM. An automated method to quantify microglia morphology and application to monitor activation state longitudinally in vivo. *PLoS One.* 2012;7(2): e31814.PMC3294422

48. Chaudhri N, Sahuque LL, Cone JJ, Janak PH. Reinstated ethanol-seeking in rats is modulated by environmental context and requires the nucleus accumbens core. *Eur J Neurosci.* 2008;28(11): 2288-2298.PMC2904679

49. Norden DM, Trojanowski PJ, Villanueva E, Navarro E, Godbout JP. Sequential activation of microglia and astrocyte cytokine expression precedes increased Iba-1 or GFAP immunoreactivity following systemic immune challenge. *Glia.* 2016;64(2): 300-316.PMC4707977

50. Chastain LG, Sarkar DK. Role of microglia in regulation of ethanol neurotoxic action. *Int Rev Neurobiol.* 2014;118: 81-103

51. Henriques JF, Portugal CC, Canedo T, Relvas JB, Summavielle T, Socodato R. Microglia and alcohol meet at the crossroads: Microglia as critical modulators of alcohol neurotoxicity. *Toxicol Lett.* 2018;283: 21-31

52. Blank T, Prinz M. Microglia as modulators of cognition and neuropsychiatric disorders. *Glia.* 2013;61(1): 62-70

53. Kohman RA. Aging microglia: relevance to cognition and neural plasticity. *Methods Mol Biol.* 2012;934: 193-218

54. Kyrargyri V, Vega-Flores G, Gruart A, Delgado-Garcia JM, Probert L. Differential contributions of microglial and neuronal IKKbeta to synaptic plasticity and associative learning in alert behaving mice. *Glia.* 2015;63(4): 549-566

55. Ransohoff RM. A polarizing question: do M1 and M2 microglia exist? *Nat Neurosci.* 2016;19(8): 987-991

56. Zhao YN, Wang F, Fan YX, Ping GF, Yang JY, Wu CF. Activated microglia are implicated in cognitive deficits, neuronal death, and successful recovery following intermittent ethanol exposure. *Behav Brain Res.* 2013;236(1): 270-282

57. Collingridge GL, Peineau S. Strippers reveal their depressing secrets: removing AMPA receptors. *Neuron.* 2014;82(1): 3-6

58. Hoogland IC, Houbolt C, van Westerloo DJ, van Gool WA, van de Beek D. Systemic inflammation and microglial activation: systematic review of animal experiments. *J Neuroinflammation.* 2015;12: 114.PMC4470063

59. Furube E, Kawai S, Inagaki H, Takagi S, Miyata S. Brain Region-dependent Heterogeneity and Dose-dependent Difference in Transient Microglia Population Increase during Lipopolysaccharide-induced Inflammation. *Sci Rep.* 2018;8(1): 2203.PMC5797160

60. McClain JA, Morris SA, Deeny MA, et al. Adolescent binge alcohol exposure induces long-lasting partial activation of microglia. *Brain Behav Immun.* 2011;25 Suppl 1: S120-128.PMC3098298

61. Buttini M, Limonta S, Boddeke HW. Peripheral administration of lipopolysaccharide induces activation of microglial cells in rat brain. *Neurochem Int.* 1996;29(1): 25-35

62. Town T, Nikolic V, Tan J. The microglial "activation" continuum: from innate to adaptive responses. *J Neuroinflammation.* 2005;2: 24.PMC1298325

63. Flatscher-Bader T, van der Brug M, Hwang JW, et al. Alcohol-responsive genes in the frontal cortex and nucleus accumbens of human alcoholics. *J Neurochem.* 2005;93(2): 359-370

64. Melendez RI, McGinty JF, Kalivas PW, Becker HC. Brain region-specific gene expression changes after chronic intermittent ethanol exposure and early withdrawal in C57BL/6J mice. *Addict Biol.* 2012;17(2): 351-364.PMC4153606

65. Morrison HW, Filosa JA. A quantitative spatiotemporal analysis of microglia morphology during ischemic stroke and reperfusion. *J Neuroinflammation.* 2013;10: 4.PMC3570327

66. Wake H, Moorhouse AJ, Jinno S, Kohsaka S, Nabekura J. Resting microglia directly monitor the functional state of synapses in vivo and determine the fate of ischemic terminals. *J Neurosci.* 2009;29(13): 3974-3980

67. Parkhurst CN, Gan WB. Microglia dynamics and function in the CNS. *Curr Opin Neurobiol.* 2010;20(5): 595-600.PMC3708473

68. Thompson KK, Tsirka SE. The Diverse Roles of Microglia in the Neurodegenerative Aspects of Central Nervous System (CNS) Autoimmunity. *Int J Mol Sci.* 2017;18(3).PMC5372520

69. Hellwig S, Brioschi S, Dieni S, et al. Altered microglia morphology and higher resilience to stress-induced depression-like behavior in CX3CR1-deficient mice. *Brain Behav Immun.* 2016;55: 126-137

70. Hinwood M, Morandini J, Day TA, Walker FR. Evidence that microglia mediate the neurobiological effects of chronic psychological stress on the medial prefrontal cortex. *Cereb Cortex.* 2012;22(6): 1442-1454

71. Tynan RJ, Naicker S, Hinwood M, et al. Chronic stress alters the density and morphology of microglia in a subset of stress-responsive brain regions. *Brain Behav Immun.* 2010;24(7): 1058-1068

72. Eyo UB, Wu LJ. Bidirectional microglia-neuron communication in the healthy brain. *Neural Plast.* 2013;2013: 456857.PMC3775394

73. Bessis A, Bechade C, Bernard D, Roumier A. Microglial control of neuronal death and synaptic properties. *Glia.* 2007;55(3): 233-238

74. Kondo S, Kohsaka S, Okabe S. Long-term changes of spine dynamics and microglia after transient peripheral immune response triggered by LPS in vivo. *Mol Brain.* 2011;4: 27.PMC3138393

75. Weinhard L, di Bartolomei G, Bolasco G, et al. Microglia remodel synapses by presynaptic trogocytosis and spine head filopodia induction. *Nat Commun.* 2018;9(1): 1228.PMC5964317

76. Biber K, Neumann H, Inoue K, Boddeke HW. Neuronal 'On' and 'Off' signals control microglia. *Trends Neurosci.* 2007;30(11): 596-602

77. Wu Y, Dissing-Olesen L, MacVicar BA, Stevens B. Microglia: Dynamic Mediators of Synapse Development and Plasticity. *Trends Immunol.* 2015;36(10): 605-613.PMC4841266

78. Wheeler D, Knapp E, Bandaru VV, et al. Tumor necrosis factor-alpha-induced neutral sphingomyelinase-2 modulates synaptic plasticity by controlling the membrane insertion of NMDA receptors. *J Neurochem.* 2009;109(5): 1237-1249.PMC2688711

79. Stellwagen D, Malenka RC. Synaptic scaling mediated by glial TNF-alpha. *Nature.* 2006;440(7087): 1054-1059

80. Pascual O, Ben Achour S, Rostaing P, Triller A, Bessis A. Microglia activation triggers astrocyte-mediated modulation of excitatory neurotransmission. *Proc Natl Acad Sci U S A.* 2012;109(4): E197-205.PMC3268269

81. Scofield MD, Kalivas PW. Astrocytic dysfunction and addiction: consequences of impaired glutamate homeostasis. *Neuroscientist.* 2014;20(6): 610-622.PMC4913887

82. Scofield MD, Heinsbroek JA, Gipson CD, et al. The Nucleus Accumbens: Mechanisms of Addiction across Drug Classes Reflect the Importance of Glutamate Homeostasis. *Pharmacol Rev.* 2016;68(3): 816-871.PMC4931870